# *Codonopis bulleynana* Forest ex Diels (cbFeD) effectively attenuates hepatic fibrosis in $CCl_4$-induced fibrotic mice model

Xiang Li [a,b,c], Yue Xing [e], Dechang Mao [e], Lu Ying [g], Yunqi Luan [f], Mei Xu [e], Hongmin Wang [e], Chunyan Li [e], Yanmei Li [e], Shuangqing Zheng [h], Zhipeng Li [h], Junbo Hu [c], Zhuoya Li [a], Huaning Wang [b,**], Yunpeng Luan [d,i,*]

[a] *Department of Immunology, School of Basic Medicine, Tongji Medical College, Huazhong University of Science and Technology, Wuhan 430030, China* [b] *Department of Pi-wei Disease, The First Affiliated Hospital of Yunnan University of Traditional Chinese Medicine, Kunming 650021, China*

[c] *Department of Gastrointestinal Surgery Center and Department of Laboratory Medicine, Tongji Hospital, Tongji Medical College, Huazhong University of Science and Technology, Wuhan, Hubei 430030, China*

[d] *Key Laboratory for Forest Resources Conservation and Utilization in the Southwest Mountains of China, Ministry of Education, Southwest Forestry University, Kunming 650224, China*

[e] *Department of Life Technology Teaching and Research, School of Life Science, Southwest Forestry University, Kunming 650224, China* [f] *Faculty of Soil Science, Department of Geography and Ecology Lomonosov Moscow State University, Russia* [g] *Yunnan Yisheng Pharmaceutical Co., Ltd., Kunming 650000, China* [h] *KPC Pharmaceuticals, Inc, Kunming 650106, China* [i] *Southwest China Eco-development Academy, Southwest Forestry University, Kunming 650224, China*

ARTICLEINFO

*Keywords:*
*Codonopis bulleynana* Forest ex Diels
Liver injury
Fibrogenesis
Inflammation
Hepatic stellate cell

ABSTRACT

The root of *Codonopis bulleynana* Forest ex Diels (cbFeD), a tonic food widely used in Yunnan Province of China, was found to have a wide range of pharmacological effects. The present study was designed to investigate the anti-fibrotic effect of water extracts of cbFeD in chronic liver injury mice model induced by carbon tetrachloride ($CCl_4$) and to explore its underlying mechanisms. Phytochemical analysis revealed multiple components were present in the water extract of cbFeD and the compounds were mostly enriched in organic acid and its derivatives, flavone, amino acid derivatives, nucleotide and its derivatives, carbohydrates etc. Treatment with cbFeD significantly attenuated liver injury and fibrosis in $CCl_4$-administered mice evidenced by improved liver histology, ameliorated apoptosis of hepatocytes, and decreased transaminase levels in the serum. Decreased activities of superoxide dismutase (SOD) and catalase (CAT) were markedly reversed upon treatment with cbFeD while levels of malondialdehyde (MDA) and glutathione (GSH) were significantly restored towards normal values. cbFeD also suppressed intrahepatic inflammatory cell infiltration and Kupffer cell activation. Furthermore, our study revealed an inhibitory effect of cbFeD on hepatic stellate cells (HSCs) activation both in vitro and in vivo. In conclusion, cbFeD could exert a protective role against liver fibrosis in mice model induced by $CCl_4$ that is comparable to the positive control silymarin and might be developed into a promising anti-fibrotic drug.

## 1. Introduction

drugs, toxic chemicals, hepatitis B or C virus infection, alcohol abuse and metabolic disorders such as nonalcoholic steatohepatitis (NASH) and Damage to the liver can be caused by various factors, for instance, autoimmune liver diseases [1]. Among these causes, chronic viral hepatitis has been the most prevalent liver disease in China. [2] Meanwhile, number of patients with NASH are also increasing due to the changes in lifestyle and dietary behaviors [3].

Persistent injury to the liver leads to dysfunction of the intrahepatic immune system and apoptosis of hepatocytes, which initiates the wound-healing response. Excessive extracellular matrix (ECM) is produced to replace the dead cells when regeneration of hepatocytes fails. [1,4] Hepatic stellate cells (HSCs) are the key cells producing ECM in the liver [5–7]. Upon stimulation by various cytokines and growth factors, HSCs undergo a phenotypic transformation from quiescent retinoid-storing cells to activated fibroblast-like cell type marked by expression of α-smooth muscle actin (α-SMA)

*Abbreviations:* NASH, nonalcoholic steatohepatitis; ECM, extracellular matrix; HSC, hepatic stellate cells; α-SMA, α- smooth muscle actin; PPAR-γ, peroxisome proliferator-activated receptor-γ;; ASH, alcoholic steatohepatitis; cbFeD, Codonopis bulleynana Forest ex diels; TCM, Traditional Chinese Medicine; $CCl_4$, carbon tetrachloride; HPF, high-power field; HRP, polymer horseradish peroxidase; TUNEL, terminal-deoxynucleotidyl transferase mediated nick end labeling; ALT, alanine aminotransferase; AST, aspartate aminotransferase; SEM, standard error of the mean; TIC, total ions chromatogram; RT, retention time; ROS, reactive oxygen species.

* Corresponding author at: Southwest China Eco-development Academy, Southwest Forestry University, Kunming 650224, China

** Corresponding author at: Department of Pi-wei disease, The First Affiliated Hospital of Yunnan University of Traditional Chinese Medicine, Kunming 650021, China.

*E-mail addresses:* zgynwhn1966@sina.com (H. Wang), 1820059756@qq.com (Y. Luan).

https://doi.org/10.1016/j.biopha.2020.110960
Received 23 March 2020; Received in revised form 28 October 2020; Accepted 1 November 2020
Available online 13 November 2020
0753-3322/© 2020 The Authors. Published by Elsevier Masson SAS. This is an open access article under the CC BY-NC-ND license (http://creativecommons.org/licenses/by-nc-nd/4.0/).

and downregulation of the peroxisome proliferator-activated receptor-γ (PPAR-γ) [8]. Activated HSCs migrate to the sites of damaged tissue, proliferate and secret type I and III collagen, and finally ECM accumulates. This breaks the original intrahepatic equilibrium of the synthesis and degradation of ECM, which may eventually disrupt normal hepatic architecture and vascularization, namely liver fibrosis [4] Progression of hepatic fibrosis is usually insidious. However, persistent fibrosis of the liver normally develops to cirrhosis which correlates with the occurrence of liver cancer as well as hepatic failure, representing a major health care burden worldwide [9–11].

Although removing etiology, e.g. anti-viral therapy for viral hepatitis or abstinence for alcoholic steatohepatitis (ASH), has shown dramatic effects on the reversal of liver fibrosis in some cases, it may by itself be insufficient for preventing progression towards cirrhosis. [12,13]To date, there is no anti-fibrogenic agent available, making liver transplantation the only curative treatment for decompensated cirrhotic liver disease [9].. As research has shown that hepatic fibrosis and early cirrhosis is completely reversible, [13] pharmacological targetings of fibrogenic pathways have been the focus of research in recent years to achieve primary prevention of hepatic fibrosis and block the occurrence of cirrhosis [14,15].

Codonopis bulleynana Forest ex Diels (cbFeD) is a perennial herb normally growing on hillside grassland and shrub at altitudes of 2800~4200 m. They are naturally distributed in Yunnan, Tibet, and Sichuan Provinces, China. [16] Roots of cbFeD, locally known as Tsoong, are popular edible Chinese herb stewed with meat by the folk of Yunnan Province long since early history. According to theories in Traditional Chinese Medicine (TCM), cbFeD exerts a modulatory effect on the immune system, digestive system, and hematologic system. Studies investigating the toxicity of cbFeD have verified that it is completely non-toxic [17]. Moreover, cbFeD is discovered to be rich in various nutrients and have a wide range of pharmacological effects [18]. Both of our previous research and others have demonstrated that cbFeD can enhance gastrointestinal peristalsis and exert an anti-constipation effect [19,20].Moreover, the immunomodulatory effect of cbFeD has been reported in different disease models [21,22]. We have reported anticancer effect of cbFeD extracts in pancreatic ductal adenocarcinoma cells as well as colorectal cancer model [23,24]. In the present study, we aimed to explore whether cbFeD could protect against liver injury and fibrosis induced by carbon tetrachloride ($CCl_4$) in mice model and the mechanism underlying its action. **2. Materials and methods**

### *2.1. Chemicals and reagents*

Carbon tetrachloride ($CCl_4$) (anhydrous, ≥ 99.5 %) was purchased from Sigma-Aldrich (St. Louis, MO, USA). Silymarin (Legalon®) was purchased from Madaus (Cologne, Germany). Primary rabbit polyclonal antibodies including anti-Collagen-I, anti-CD45, anti-F4/80, anti- α-SMA, anti-desmin and anti-PPAR-γ, secondary goat anti-rabbit immunoglobulins/HRP (Ig Fraction) antibody were purchased from Servicebio (Wuhan, China). Haematoxylin and eosin (H&E) and diaminobenzidine (DAB) from the Wuhan Servicebio Technology Co., Ltd. (Wuhan, China). Commercial diagnostic kits of alanine aminotransferase (ALT) and aspartate aminotransferase (AST) were purchased from BioSino Biotechnology and Science Co., Ltd. (Beijing, China). Superoxide dismutase (SOD), catalase (CAT), malondialdehyde (MDA) and glutathione (GSH) assay kits were purchased from Nanjing Jiancheng Bioengineering Institute (Nanjing, China).

### *2.2. Plant materials and extract procedures*

The fresh roots of cbFeD were collected from Xundian, Yunnan Province, China.

The plants were identified and authenticated by academician Deyuan Hong, State Key Laboratory of Systematic and Evolutionary Botany, Institute of Botany, Chinese Academy of Sciences, Beijing, China.

Water extract of cbFeD was prepared following our previous procedure [19,23]. Briefly, 100 g fresh root of cbFeD were cut into thin slices and decocted three times with 1:10 (w/v) distilled water for 30 min. The filtrate was collected and concentrated under reduced pressure at 50℃ to a final volume of 50 mL. Water extract of cbFeD was obtained by this preparation at a concentration of 2 g/mL crude drug and then stored at -20℃.

### *2.3. LC-ESI-MS/MS analysis of water extract of cbFeD*

200 μL water extract of cbFeD was mixed overnight at 4 ◦C with 1.0 mL 70 % aqueous methanol containing 0.1 mg/L lidocaine for internal standard. Following centrifugation at 10 000 *g* for 10 min, the supernatant were absorbed and filtrated (SCAA-104, 0.22-μm pore size; ANPEL, Shanghai, China, www.anpel.com.cn/) before LC–MS/MS analysis.

The compounds extracted were analyzed using an LC-ESI-MS/MS system (UPLC, Shim-pack UFLC SHIMADZU CBM30A, http://www.sh imadzu.com.cn/); MS/MS (Applied Biosystems 6500 QTRAP, http:// www.appliedbiosystems.com.cn/).

A volume of 2 μl sample was injected onto a Waters ACQUITY UPLC HSS T3 C18 column (2.1 mm × 100 mm, 1.8 μm) operating at 40 ◦C and a flow rate of 0.4 mL/min. The mobile phases used were acidified water (0.04 % acetic acid) (Phase A) and acidified acetonitrile (0.04 % acetic acid) (Phase B). Compounds were separated using the following gradient: 95:5 Phase A/Phase B at 0 min; 5:95 Phase A/Phase B at 11.0 min; 5:95 Phase A/Phase B at 12.0 min; 95:5 Phase A/Phase B at 12.1 min; 95:5 Phase A/Phase B at 15.0 min. The effluent was connected to an ESI-triple quadrupole-linear ion trap (Q TRAP)–MS. LIT and triple quadrupole (QQQ) scans were acquired on a triple quadrupole-linear ion trap mass spectrometer (Q TRAP), AB Sciex QTRAP6500 System, equipped with an ESI-Turbo Ion-Spray interface, operating in a positive ion mode and controlled by Analyst 1.6.1 software (AB Sciex). The operation parameters were as follows: ESI source temperature 500 ◦C; ion spray voltage (IS) 5500 V; curtain gas (CUR) 25 psi; the collision- activated dissociation (CAD) was set highest. QQQ scans were acquired as MRM experiments with optimized declustering potential (DP) and collision energy (CE) for each individual MRM transitions. The *m/z* range was set between 50 and 1000.

To produce a matrix containing fewer biased and redundant data, peaks were checked manually for signal/noise (s/n) > 10 and in-house software written in Perl was used to remove the redundant signals caused by different isotopes, in-source fragmentation, K+, Na+, and NH4+ adduct, and dimerization. To facilitate the identification/annotation of metabolites, accurate *m/z* for each Q1 was obtained. Total ion chromatograms (TICs) and Extracted Ion Chromatogram (EICs or XICs) of QC samples were exported to give an overview of metabolite profiles of all samples. The area of each chromatographic peak was calculated. Peaks were aligned

across the different samples based on spectral pattern and retention time. Metabolites were identified by searching internal database and public databases (MassBank, KNApSAcK, MoTo DB, and METLIN) and comparing the *m/z* values, the RT, and the fragmentation patterns with the standards.

### *2.4. Animals and treatment*

Healthy male KM mice (SPF-grade, 6-week-old, 20–25 g) were purchased from Hunan SJA Laboratory Animal Co., Ltd (Hunan, China). The animals were housed six per cage on paper chip bedding in a barrier room with controlled temperate (22.0 ± 2℃), humidity (50 %–60 %), free access to autoclaved food and drinking water, an alternating 12 -h light and dark cycle. All experimental manipulations were carried out in accordance with the guidelines of the Chinese Council for Animal Care. All animal studies were approved by the Kunming Animal Care and Use Committee.

After acclimation for one week, the animals were randomized into four groups (with 6 mice per group) including normal control group (Control), model group ($CCl_4$), the silymarin treated group ($CCl_4$+Silymarin) and the cbFeD treated group ($CCl_4$+cbFeD). Normal control group received corn oil at 0.05 mL/10 *g* BW via orogastric gavage whereas mice in the rest three groups were intragastrically administered with 40 % $CCl_4$ in corn oil vehicle (v/v, 0.05 mL/10 *g* BW) to induce chronic liver injury and fibrogenesis. The intragastric gavage of corn oil or $CCl_4$ solution were administered twice a week for 7 consecutive weeks. Mice in the silymarin treated group were gavaged daily with silymarin dissolved in 0.5 % CMC-Na (at a dosage of 50 mg/kg BW). Water extracts of cbFeD were dissolved in advance with distilled water and administered to the mice in cbFeD-treated group by gavage (at a dosage of 1 *g*/kg BW). Meanwhile, mice in the control group and model group were given the same volume of distilled $H_2O$ through intragastric gavage every day (0.05 mL/10 *g* BW). The treatment started from the fourth week until study completion. 3 days after the last dose of $CCl_4$ or vehicle all the experimental mice were fasted for 24 h and then euthanized by pentobarbital sodium (45 mg/kg, i.p.). Blood samples were collected from retro-orbital sinus by removing the eyeballs and left at 4 ℃ for an hour followed by centrifugation at 4 ℃, 3000 rpm/min for 15 min to obtain serum. Serum was frozen at − 80 ℃ for further analysis. Livers were excised, weighed and photographed before partly fixed in 4% buffered paraformaldehyde for histological analysis and partly frozen in liquid nitrogen immediately. The liver samples in the liquid nitrogen were subsequently transferred to ultra-low temperature freezer and stored at − 80 ℃ until analysis. The ratios of liver to body weight were calculated as follows:

$$\text{The ratios of liver to body weight} = \text{liver weight (g)/body weight (g)} \times 100\ \%$$

### *2.5. Histological and immunohistochemical analysis*

Fixed liver specimens from the same part of the lobe of liver in 4% buffered paraformaldehyde for over 24 h, were dehydrated with different graded alcohol series, embedded in paraffin and cut into 5 μm thick sections. The sections were performed with hematoxylin and eosin (H&E) staining for histological observation or with 0.2 % Sirius red staining to quantitatively assess extent of collagen deposition. Masson' s trichrome staining were also performed with tissue sections for the assessment of collagen contents in the livers. The stained sections were examined under microscope (Nikon DS-U3, Japan) and documented by Q-Captuter Pro system. The percentage of area of positive Sirius Red staining in the liver was measured under five random high-power (400×) fields (HPF) per slide and analyzed by Image-pro Plus 6.0. The observation and analysis were performed in a blinded fashion to the group distribution with two observers.

Deparaffinized liver sections were immersed in distilled water at room temperature for 25 min and blocked with 3% rabbit serum for 30 min. Then the primary antibody was added and incubated overnight at 4 ℃. After being washed with PBS, the tissue slides were then labeled with polymer horseradish peroxidase (HRP) secondary antibody for 1.5 h at room temperature, followed by DAB staining and dehydrated sealing. Slides were observed under microscope. Positively-stained areas in the liver was measured under five random high-power (200×) fields per slide and then calculated by Image-pro Plus 6.0. Positive cells are counted respectively under five random high-power fields (200×) per slide and expressed as mean positive cells/HPF. The observer was blinded to the group distribution when the analyses were made.

### *2.6. Measurements of apoptosis by TUNEL*

Apoptosis of the cells in the liver was detected by terminal-deoxynucleotidyl transferase mediated nick end labeling (TUNEL) staining (Boster Biological Technology Co. Ltd., Wuhan, China) according to the manufacturer's protocol. Nuclei were counterstained with 4, 6-diamidino2-phenylindole (DAPI) in the same sections. Cells were evaluated using fluorescence microscopy (Nikon Eclipse C1). Apoptotic cell in the liver indicated by co-location of TUNEL and DAPI staining was counted under five random high-power (200×) fields per slide. The observer was blinded to the group distribution when the analyses were made.

### *2.7. Determination of serum transaminase levels*

Serum levels of alanine aminotransferase (ALT) and aspartate aminotransferase (AST) were analyzed using commercial kits according to manufacture's instructions. *2.8. Assessment of oxidative stress*

Each liver tissue sample from mice of individual experiment group was homogenized with ice-cold normal saline in a 1:9 ratio (w/v, liver: saline) and centrifuged at 3000 rpm (4 ℃) for 15 min. The supernatant was used to measure the activity of SOD, CAT and the level of MDA, GSH using the commercial standardized kits according to the manufacturer's instructions.

### *2.9. Immunofluorescence analysis*

Liver sections were immunostained with α-SMA rabbit polyclonal antibody overnight at 4 ℃ followed by incubation with CY3–conjugated goat anti-rabbit secondary antibody at room temperature for 50 min in dark condition. Then DAPI solution was added to counterstain the nucleus at room temperature for 10 min in dark place. The sections were sealed with anti-fade mounting medium and visualized using a fluorescence microscope (Nikon Eclipse C1). DAPI glows blue by UV excitation wavelength 330− 380 nm and emission wavelength 420 nm; CY3 glows red by excitation wavelength

510− 560 nm and emission wavelength 590 nm. The α-SMA positive cells in the liver was counted under five random high-power (200×) fields per slide and documented by Q- Captuter Pro system. The observer was blinded to the group distribution when the analyses were made.

### 2.10. Cell culture

LX2, a human HSC cell line cells were obtained from the Type Culture Collection of the Chinese Academy of Sciences (Shanghai, China), and were maintained in DMEM with 10 % FBS at 37 °C in an atmosphere with 5% $CO_2$.

### 2.11. Cell viability assay

LX2 cells were seeded in 96-well plates in triplicate at a density of 2.0 × $10^3$/well and cultured overnight for cells to adhere and attach. Then LX2 cells were treated with TGF-β1 (10 ng/mL) and water extract of cbFeD at indicated concentrations (100, 200, 400ug/mL) for 24 h. Cell viability was tested by CellTiter 96® AQueous One solution (20 μL/well) and the absorbance at 490 nm was measured after 4 h of incubation at 37 °C.

### 2.12. Protein extraction and western blot analysis

LX-2 cells were treated with TGF-β1 (10 ng/mL) and water extract of cbFeD at indicated concentrations for 24 h. Cells were lysed with RIPA (Beyotime, Jiangsu, China) and PMSF (Beyotime, Jiangsu, China) lysate buffer. The protein concentration was measured with the bicinchoninic acid (BCA) assay kit (Beyotime, Jiangsu, China) according to the manufacturer's instruction. Then equal amount of each

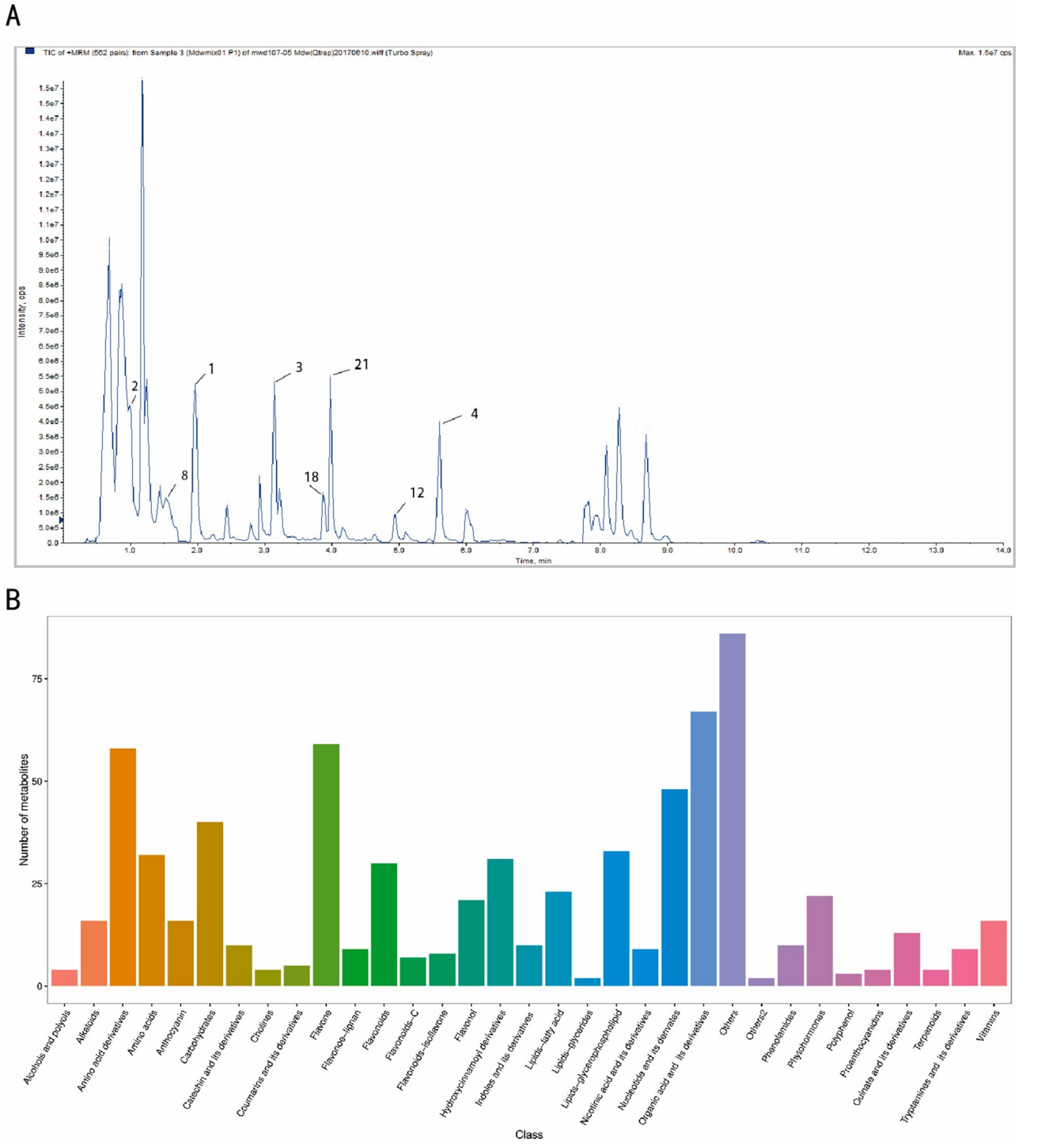


**Fig. 1.** LC-ESI-MS/MS analysis of water extract of cbFeD. (A) Base peak chromatogram using the positive ionization mode of the water extract of cbFeD obtained by LC-ESI-MS/MS analysis. (B) Classification of the identified metabolites from the water extract of cbFeD.

sample protein was separated using 10 % sodium dodecyl sulfate-polyacrylamide gel (SDS-PAGE) electrophoresis and transferred to polyvinylidene fluoride (PVDF) membranes. Next, nonspecific proteins were blocked with TBS/ Tween 20 (0.075 %) solution containing 5% skim milk for 3 h at room temperature. The PVDF membranes were washed 3 times with TBS/ Tween20 and each time for 15 min before incubated with individual primary antibody (α-SMA, Collagen I, PPAR-γ) and β -actin as an internal control at 4 °C overnight. The membranes were washed 3 times with TBS/Tween 20 and each time for 15 min, then incubated with secondary

antibodies at room temperature for 1 h. Target protein bands were visualized using the Tanon 5200 Multi-Chemiluminescent Imaging System (Tanon Science & Technology Co., Ltd, Shanghai, China) and quantitatively analyzed using the Image Lab software (Bio-Rad, USA).

### 2.13. Statistical analysis

Data are expressed as mean ± standard error of the mean (SEM). Differences between groups were assessed using the unpaired two-tailed Student's *t*-test or one way analysis of variance (ANOVA). $P < 0.05$ was considered statistically significant. The analysis was performed with SPSS version 16.0 (SPSS Inc., Chicago, IL) statistical software, and graphs were created using GraphPad Prism version 6.0 (GraphPad Software Inc., San Diego, CA) software.

## 3. Results

### 3.1. Phytochemical analysis of the water extract of cbFeD

The phytochemical analysis was conducted to characterize the composition of the water extract of cbFeD by LC-ESI-MS/MS analysis. Fig. 1A depicts the total ions chromatogram (TIC) in the positive ionization mode. Hundreds of compounds were identified and their molecular formulae were generated based on accurate mass measurements, comparison of MS/MS fragmentation pattern with information retrieved from multiple public databases (MassBank, KNApSAcK, MoTo DB, and METLIN). The classifications of these compounds enriched in organic acid and its derivatives, flavone, amino acid derivatives, nucleotide and its derivatives, carbohydrates, etc (Fig. 1B). A total of 30 representative components were listed in Table 1 and Fig. 2, which provided information on retention time (RT), molecular formula, name, classification, the relative content, and molecular structure of these compounds.

### 3.2. cbFeD dramatically reduced liver injury in mice subjected to chronic $CCl_4$-intoxication

Fig. 3A is a schematic illustration of our experiment. The liver of each mice was photographed and weighed immediately after euthanization and representative photos were shown in Fig. 3B. Chronic $CCl_4$-administration resulted in liver enlargement and fibrosis manifested by a pale, dry, and abnormal pattern on the surfaces while treatment with silymarin or water extract of cbFeD alleviated these changes. Per the macroscopic view of the liver specimen, a significant increase in the ratios of the liver to body weight was observed in the $CCl_4$-induced fibrotic model group compared to that of the control group ($P < 0.01$). The ratios of the liver to body weight were restored in mice treated with silymarin or cbFeD extracts compared to the model group ($P < 0.01$) (Fig. 3C). During the experiment period, the body weight of mice in each group was monitored and mice in the fibrosis model group showed a decreased in body weight compared to that of the control mice since the 5th week and this decrease in body weight lasted till the end of the experiment. However, treatment with silymarin or cbFeD extracts partially restored this decrease in body weight (Fig. 3D). Histological changes of liver were investigated and HE-stained liver sections exhibited areas of necrosis, steatosis, ballooning of hepatocytes, and inflammatory infiltration, which are the hallmarks of hepatic injury in $CCl_4$-induced fibrotic model mice (Fig. 3E). Liver sections from cbFeD or silymarin treated animals, however, showed a noticeable amelioration of these changes, suggesting attenuation of hepatic injury and inflammation. These results supported a protective effect of cbFeD against $CCl_4$-induced liver injury.

### 3.3. cbFeD attenuated hepatic fibrosis

To evaluate hepatic fibrosis, Masson Trichome, and Sirius red staining of liver sections were carried out. As Fig. 4A showed, liver

sections of the $CCl_4$-induced fibrotic model group exhibited areas of fibrosis in the centrilobular and perilobular region. Quantitative

**Table 1**

| Index | Rt (min) | Molecular Formula | Compounds | Classification | Percent (%) |
|---|---|---|---|---|---|
| 1 | 1.95 | $C_6H_6N_4S$ | 6-Methylmercaptopurine | Nucleotide and its derivates | 3.405 |
| 2 | 0.74 | $C_6H_{12}O_6$ | Myoinositol | Alcohols and polyols | 3.132 |
| 3 | 3.12 | $C_{17}H_{20}N_4O_6$ | Vitamin B2 | Vitamins | 2.440 |
| 4 | 5.56 | $C_{16}H_{12}O_6$ | Chrysoeriol | Flavone | 1.652 |
| 5 | 2.81 | $C_{15}H_{14}O_6$ | Catechin | Catechin and its derivatives | 1.625 |
| 6 | 0.83 | $C_{17}H_{16}O_4$ | Demethoxymatteucinol | Coumarins and its derivatives | 1.037 |
| 7 | 3.21 | $C_{16}H_{18}O_4$ | 3,4-DiMethoxy-6-phenethylbenzene-1,2-diol | Alkaloids | 0.645 |
| 8 | 1.5 | $C_{10}H_{13}N_5O_5$ | Crotonoside | Others | 0.595 |
| 9 | 0.79 | $C_5H_{14}NO$ | Choline | Cholines | 0.373 |
| 10 | 5.58 | $C_{22}H_{22}O_{11}$ | Tricin | Flavone | 0.334 |
| 11 | 2.69 | $C_{16}H_{18}O_9$ | Chlorogenic acid | Quinate and its derivatives | 0.301 |
| 12 | 4.83 | $C_{15}H_{10}O_6$ | Orobol | Flavonoids-isoflavone | 0.206 |
| 13 | 4.91 | $C_{15}H_{10}O_6$ | Luteolin | Flavone | 0.181 |
| 14 | 0.59 | $C_6H_8O_6$ | L-Ascorbic Acid | Vitamins | 0.174 |
| 15 | 3.7 | $C_{21}H_{20}O_{11}$ | Cynaroside | Flavone | 0.108 |
| 16 | 5.48 | $C_{15}H_{10}O_5$ | Apigenin | Flavone | 0.055 |
| 17 | 7.32 | $C_{20}H_{20}O_7$ | Tangeretin | Flavone | 0.037 |
| 18 | 3.86 | $C_{22}H_{24}O_{11}$ | Hesperetin 5-O-glucoside | Flavonoids | 0.020 |
| 19 | 5.41 | $C_{15}H_{12}O_5$ | Naringenin | Flavonoids | 0.020 |
| 20 | 0.8 | $C_{12}H_{22}O_{11}$ | Trehalose | Carbohydrates | 0.017 |
| 21 | 3.99 | $C_{28}H_{34}O_{15}$ | Hesperidin | Flavone | 0.017 |
| 22 | 4.26 | $C_{21}H_{20}O_{12}$ | Quercetin-3-beta-O-galactoside | Flavonol | 0.016 |
| 23 | 3.73 | $C_{27}H_{30}O_{16}$ | Quercetin 7-O-rutinoside | Flavonol | 0.015 |

24 )14
25 )09
26 )08
27 )03
28 )03
29 )02
30 )02

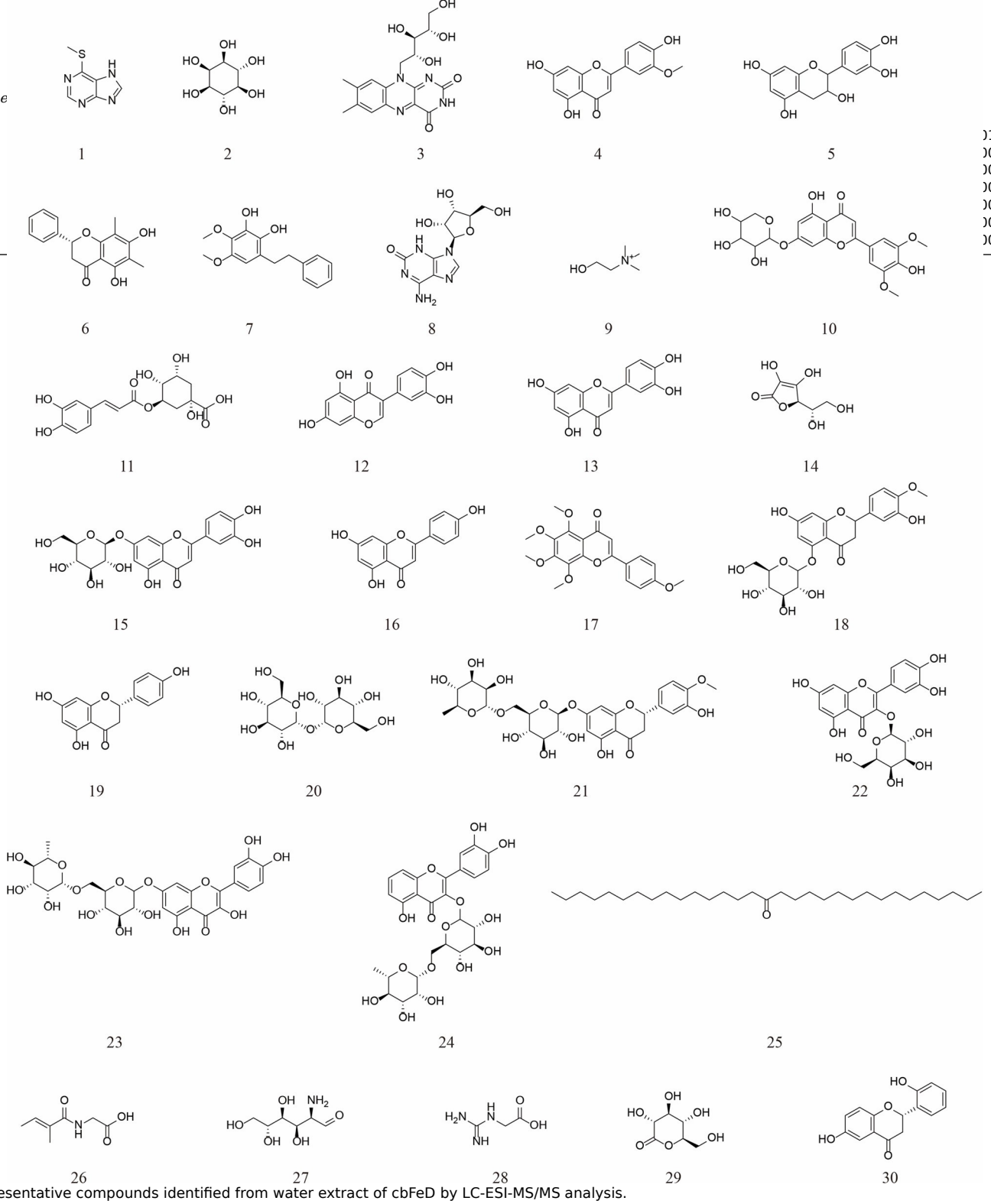


Representative compounds identified from water extract of cbFeD by LC-ESI-MS/MS analysis.

**Fig. 2.** Structure of the representative compounds identified from the water extract of cbFeD obtained by LC-ESI-MS/MS analysis. Compounds are numbered according to Table 1.

analysis using Image Pro-Plus corroborated this increase showing an increased percentage of blue-stained area per HPF upon repeated exposure to $CCl_4$ compared to the control group (3.17 ± 0.16 versus 0.034 ± 0.02, respectively; $P < 0.001$). (Fig. 4A, C), whereas liver sections from mice treated with cbFeD showed marked reduction in the fibrotic area compared to the model group (0.22 ± 0.04 versus 3.17 ± 0.16, respectively; $P < 0.01$). Liver sections from mice treated with silymarin exhibited an obvious reduction in fibrosis compared with the model group (0.72 ± 0.04 versus 3.17 ± 0.16, respectively; $P < 0.01$). However, there was no significant difference in the fibrotic area between cbFeD and silymarin treatment ($P > 0.05$). Sirus red staining showed similar results on the fibrosis of the liver tissue between different groups.

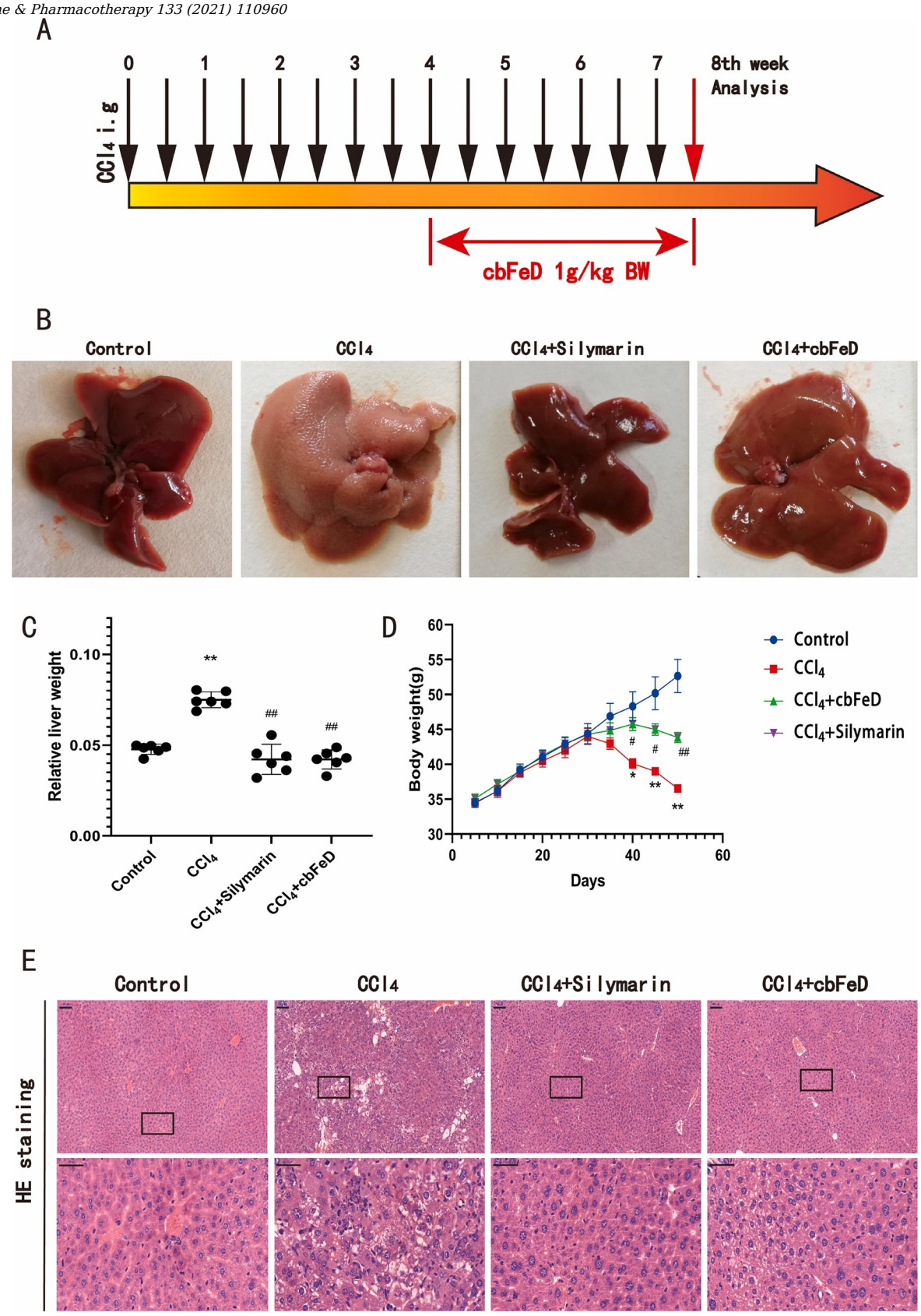


**Fig. 3.** cbFeD treatment reduced liver injury in $CCl_4$ administered mice. (A) Graphic illustration of the experiment design. (B) Representative photograph of livers from each experiment group under macroscopic view. (C) Mice and their liver samples were weighted and liver to body weight ratio were calculated. (D) Body weight change throughout the experiment. (E) Representative histology of liver tissue from each group by H&E staining under light microscopy at 100× and 400× magnifications. Scale bar = 50 μm. Control, normal control group; $CCl_4$, $CCl_4$-induced liver injury

and fibrosis model group; $CCl_4$ + Silymarin, silymarin treated group ; $CCl_4$+cbFeD cbFeD treated fibrotic group. (*) $P < 0.05$, significantly different compared to the control group; (**) $P < 0.01$, significantly different compared to the control group; (#) $P < 0.05$, significantly different compared to the $CCl_4$ group; (##) $P < 0.01$, significantly different compared to the $CCl_4$ group.

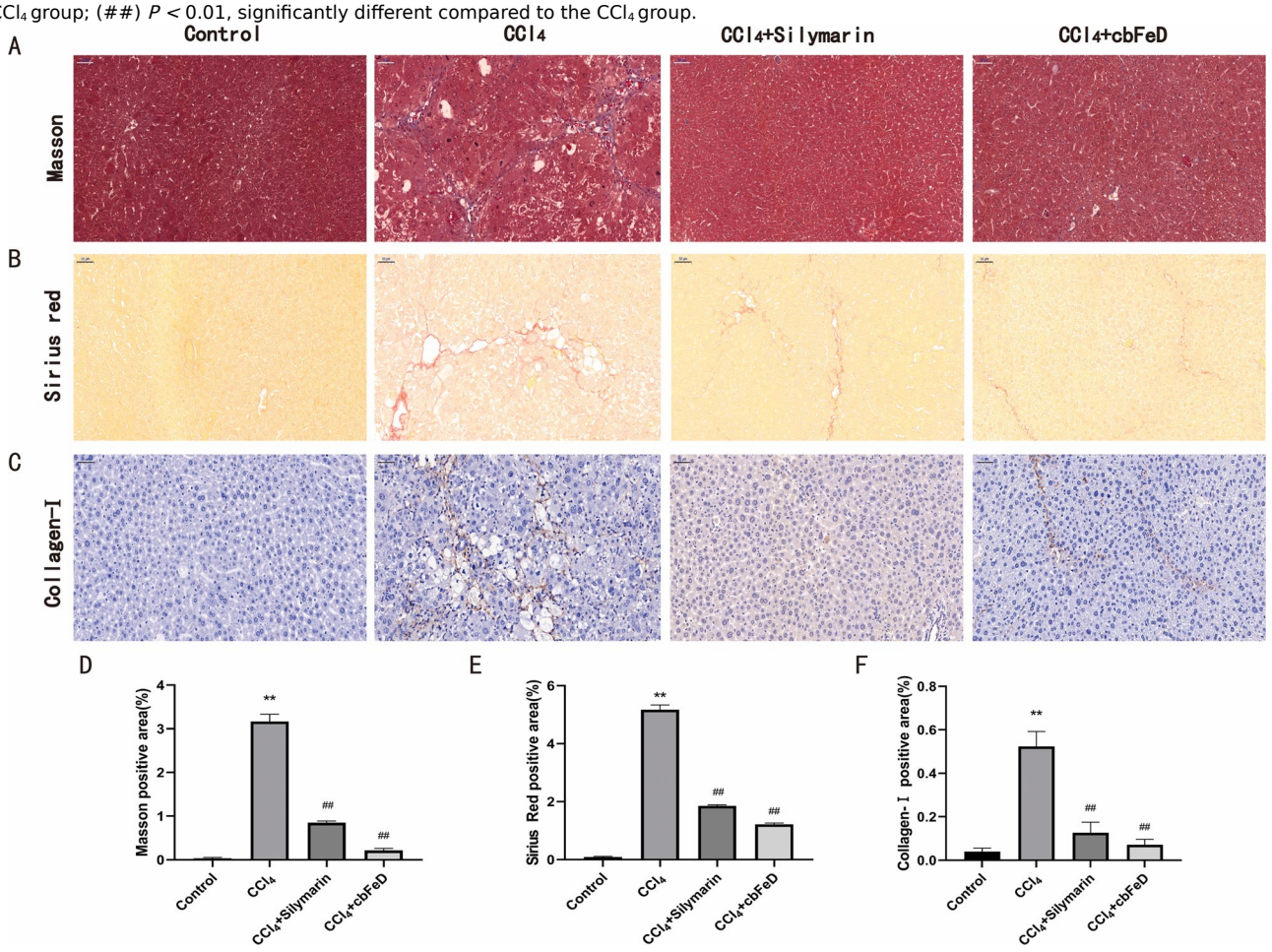


**Fig. 4.** cbFeD treatment attenuated hepatic fibrosis. Collagen deposition in the liver in each group by Masson' s trichrome staining (A) and Sirius Red staining (B). (C) Collagen-I deposition in the liver sections from each group by IHC. Magnification ×200. Scale bar = 50 μm. (D to F) Quantitative analysis of positive stained area respectively using Image Pro-Plus. The data are based on the examination of five random high power fields. Results are expressed as the mean ± SEM; (**) P < 0.01, significantly different compared to the control group; (##) P < 0.01, significantly different compared to the $CCl_4$ group.

We further observed Collagen-I deposition in liver sections via immunohistochemical staining. cbFeD treatment resulted in a significant decrease in collagen-I deposition quantified by positively-stained areas per HPF (0.072 ± 0.02) compared to the model group (0.524 ± 0.07) (P < 0.001) while collagen-I was hardly seen in liver sections of control mice (0.04 ± 0.02). (Figs. 4B, D). These results suggested that cbFeD could attenuate $CCl_4$-induced hepatic fibrosis.

### *3.4. cbFeD ameliorated apoptosis of hepatocytes and lowered serum transaminases*

Cell apoptosis in the liver was assessed by the TUNEL assay and co- location of TUNEL and DAPI staining in the nucleus indicated apoptotic cells. As shown in Fig. 5A, apoptotic cells was occasionally observed in the liver sections from the control group under fluorescence microscopy. However, a significant increase in cell apoptosis were seen in the liver sections from the $CCl_4$-induced model group. Fewer apoptotic cells were observed in liver sections in both the silymarin and cbFeD treated groups compared with that from the $CCl_4$-induced model group. The numeration of TUNEL-positive cells in each group revealed that the number of apoptotic cells was 1.2 ± 0.4 cells/HPF in the control group, 12.2 ± 1.9 cells/ HPF in the $CCl_4$ model group, 6.3 ± 2.4 cells/ HPF in the silymarin treated group and 3.4 ± 1.1 cells/HPF in cbFeD treated group respectively. Number of apoptotic cells in the cbFeD treated group was significantly lower compared to that of the $CCl_4$ model group ($P < 0.01$) (Fig. 5B). Serum ALT and AST, the most sensitive and commonly used biomarkers of liver injury, are elevated in the blood when damage of the parenchyma cells in the liver occurs. We measured levels of ALT and AST in the serum of experiment mice and found that the activity of both these enzymes increased nearly two folds in mice of the model group compared to that of the control ($P < 0.01$). A significant inhibition of this elevation ($P < 0.01$) was observed in both the silymarin and cbFeD treated group (Fig. 5C, D). Overall, these results supported the hepatoprotective effects of cbFeD by attenuating hepatocyte apoptosis and lowering transaminase levels during the process of liver injury which was comparable with silymarin.

### 3.5. cbFeD attenuated oxidative stress in the liver

$CCl_4$ caused oxidative stress in mice model indicated by the significant increase in MDA level (Fig. 6A). Antioxidant enzyme SOD and CAT were also analyzed, and both were observed to have a dramatic reduction (Fig. 6B and C). Depleted hepatic GSH content was observed compared with the control group (Fig. 6D). Treatment with silymarin as well as cbFeD effectively attenuated the oxidative stress, such as lowering MDA and increasing the activity of SOD and CAT. Besides, GSH content was also restored significantly compared to the model group.

### 3.6. cbFeD suppressed intrahepatic Leukocyte Recruitment and Kupffer Cell activation

Since inflammation is considered a prerequisite and important co-

**Fig. 5.** cbFe ected by TUNEL as ers of positive stai T (D) levels in the ferent compared to

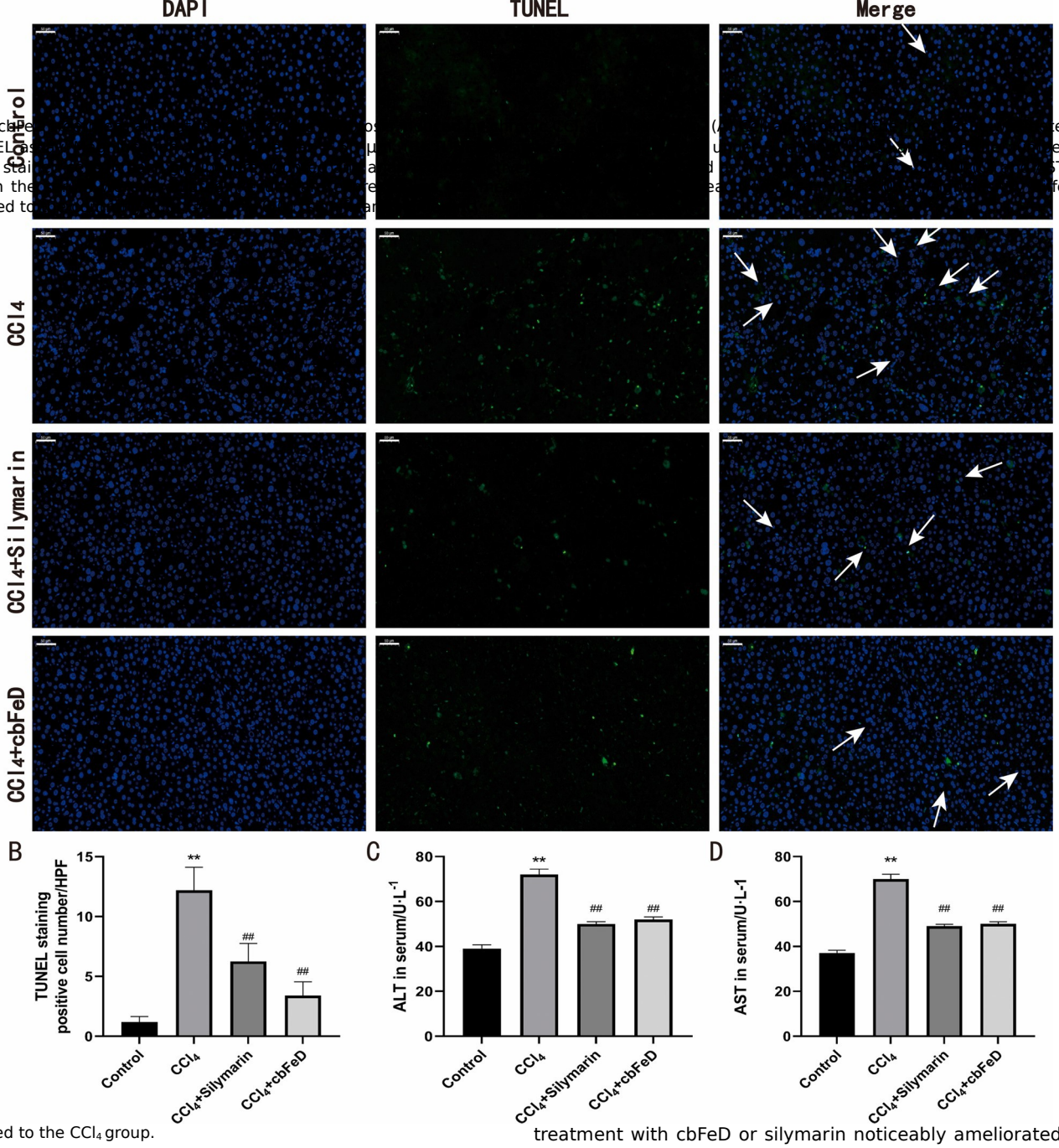


compared to the $CCl_4$ group.

contributor to fibrosis, we evaluated the inflammatory infiltration and activation of Kupffer cells induced by $CCl_4$-mediated liver injury. Immunostaining with an anti-CD45 antibody was performed in liver sections to investigate leukocyte infiltration. As showed in Fig. 7A, CD45 positive cells were hardly seen in the control group. However, in the $CCl_4$-induced model group, a significant increase in the number of CD45 positive cells were observed, especially in the periportal area. Treatment with cbFeD or silymarin dramatically reduced CD45 positive cell number. Numeration of CD45 positive cells under 5 random HPF in sections from each group were illustrated in Fig. 6C which revealed significantly more CD45 positive cell infiltration in $CCl_4$-induced model group compared with the control group ($P < 0.01$) and a dramatic reduction in the number of CD45 positive cells in the cbFeD-treated group compared with the model group ($P < 0.01$). Moreover, Kupffer cell activation was evaluated through IHC staining of its marker F4/80. The number of F4/ 80 positive cells increased dramatically in liver sections from fibrotic model group and treatment with cbFeD or silymarin noticeably ameliorated the increase in the number of activated Kupffer cells (Fig. 7B, D). These results have suggested the suppressive effect of cbFeD on inflammatory response during hepatic fibrosis.

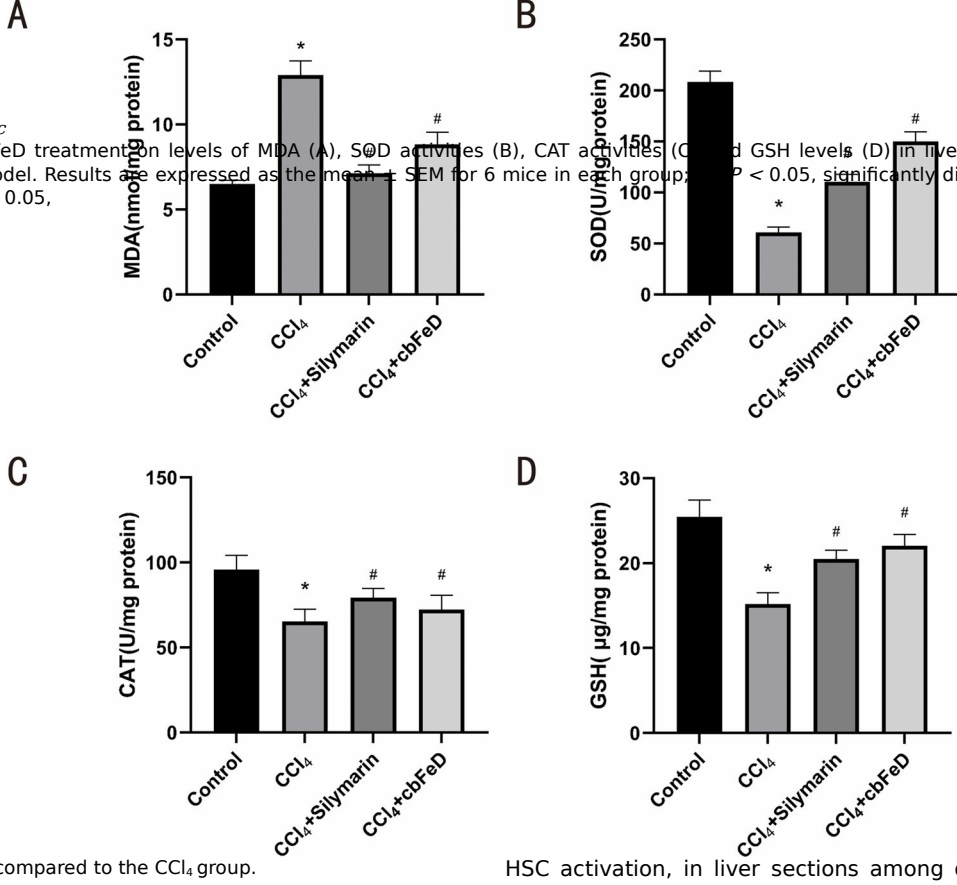


**Fig. 6.** Effects of cbFeD treatment on levels of MDA (A), SOD activities (B), CAT activities (C) and GSH levels (D) in liver tissue of $CCl_4$-induced chronic liver injury model. Results are expressed as the mean ± SEM for 6 mice in each group; (*) $P < 0.05$, significantly different compared to the control group; (#) $P < 0.05$, significantly different compared to the $CCl_4$ group.

### *3.7. cbFeD inhibited the Activation of HSCs in vivo*

Since activated HSCs are the major source of ECM production and play a vital role in liver fibrogenesis, we investigated the effect of cbFeD on the activation of HSCs induced by $CCl_4$. As shown in Fig. 8A and C, immunofluorescent staining of α-SMA revealed a dramatic increase in α-SMA expression in the $CCl_4$-induced model group compared with the control group ($P$ <0.001) while expression of α-SMA in cbFeD treatment group or silymarin treated group decreased significantly ($P < 0.001$). In addition, desmin, another commonly used marker of the activated HSCs, was also examined in our experiment by IHC. The expression of desmin was induced upon $CCl_4$ administration and less detected in cbFeD or silymarin treated group (Fig. 8B). The number of desmin positive cells was further enumerated and illustrated in Fig. 7D. These data provided powerful evidence for the inhibitory effect of cbFeD on HSC activation.

### *3.8. cbFeD inhibited the Activation of HSCs in vitro*

The effect of cbFeD on the activation of HSCs were further investigated in vitro. As shown in Fig. 9A, cell viability assay revealed a dramatic increase in cell viability of LX2 cells upon TGF-β1 (10 ng/mL) stimulation. However, a dose-dependent inhibition of cbFeD on the viability of TGF-β1stimulated LX2 cells were observed. We then assessed the fibrotic markers of HSC activation by western blot analysis. A significant increase in α-SMA and collagen-I expression and a dramatic decrease in PPAR-γ expression were observed in LX2 cells upon TGF-β1 (10 ng/mL) stimulation compared with the control cells ($P < 0.01$). cbFeD treatment at indicated concentrations significantly restored these changes ($P < 0.01$, Fig. 9B). We further evaluated expression of PPAR-γ, a key molecule modulating HSC activation, in liver sections among different experiment groups by IHC staining. As illustrated in Fig. 9C, PPAR-γ is highly expressed in mesenchymal cells of the control group. Notably, expression of PPAR-γ dramatically reduced in the $CCl_4$ treated model group. Restoration of PPAR-γ was observed in the liver section of cbFeD or silymarin treated group. These results further supported the inhibitory effect of cbFeD on HSC activation.

## 4. Discussion

The present study was aimed to determine the effect of cbFeD on chronic liver injury and fibrogenesis in a murine model induced by chronic $CCl_4$-administration. We demonstrated that the application of water extracts of cbFeD effectively attenuated liver injury and fibrosis. To our knowledge, this is the first study showing the positive effects of cbFeD on hepatic fibrosis which reveals its potential in the development of anti-fibrotic drugs.

As the most widely used hepatotoxic agent to induce liver injury animal models, $CCl_4$ increases free radicals and reactive oxygen species (ROS) formation which subsequently causes lipid peroxidation of membranous structures and apoptosis of hepatocytes. [25] In our research treatment with cbFeD significantly attenuated damage to the liver and reduced the number of apoptotic hepatocytes manifested by liver sections stained with HE and TUNEL respectively. Levels of ALT and AST, two sensitive indicators of hepatocyte integrity, which showed a dramatic increase upon $CCl_4$-induced liver injury, were observed to restore significantly after treatment with cbFeD. Moreover, cbFeD treatment effectively attenuated the oxidative stress comparable with silymarin treatment, such as lowering MDA, increasing the activity of SOD and CAT, and restoring GSH content in the liver tissue. These results indicated that cbFeD could enhance the antioxidant capability,

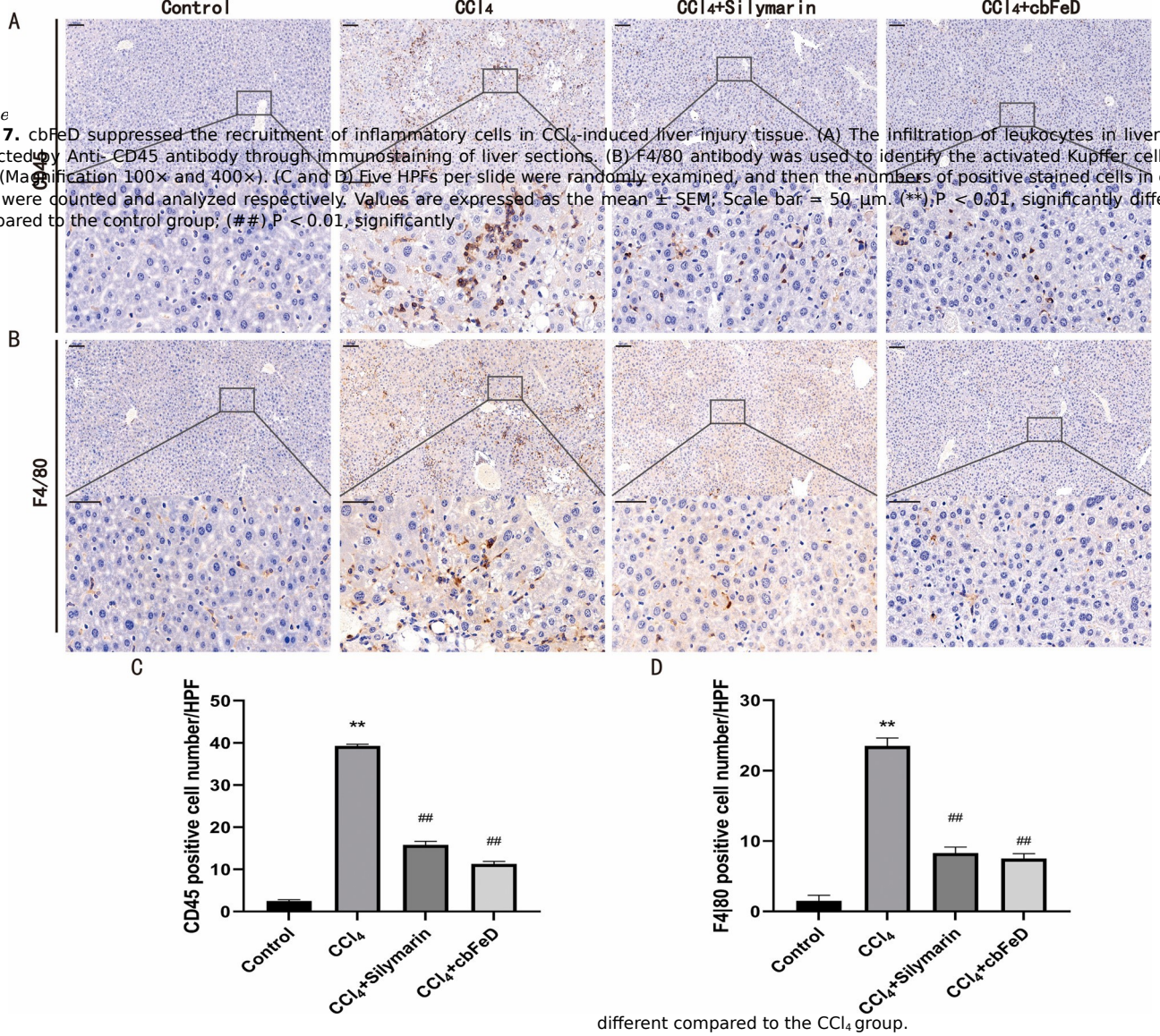


**Fig. 7.** cbFeD suppressed the recruitment of inflammatory cells in $CCl_4$-induced liver injury tissue. (A) The infiltration of leukocytes in liver was detected by Anti- CD45 antibody through immunostaining of liver sections. (B) F4/80 antibody was used to identify the activated Kupffer cells by IHC. (Magnification 100× and 400×). (C and D) Five HPFs per slide were randomly examined, and then the numbers of positive stained cells in each field were counted and analyzed respectively. Values are expressed as the mean ± SEM; Scale bar = 50 μm. (**),$P < 0.01$, significantly different compared to the control group; (##),$P < 0.01$, significantly different compared to the $CCl_4$ group.

ameliorate lipid peroxidation and prevent the damage of liver tissue induced by $CCl_4$.

According to the phytochemical analysis of the water extracts from cbFeD in our work, hundreds of chemicals were identified and enriched in organic acid and its derivatives, flavone, amino acid derivatives, nucleotide and its derivatives, carbohydrates etc. Liu et al. analyzed the nutritional components of cbFeD and conclude that cbFeD was well balanced in nutrition that was rich in amino acids, vitamins and polysaccharides [18]. They further studied the reducing capacity and scavenging activity of the polysaccharides extracted from cbFeD for free radical DPPH, ·OH and $O^{2-}$ and concluded that the polysaccharides from cbFeD possess excellent anti-oxidant activity [26]. Flavonoids are another class of bioactive constituents found abundantly in the root of cbFeD which are well-known for their antioxidant and hepatoprotective effects [27–31]. More and more efforts have been devoted to the isolation, structural identification and biological evaluation of the effective compounds from the extracts of the root of cbFeD, deepening our understanding of its pharmacological effects [32–35]. Further identification of the components responsible for the hepatoprotective effect of cbFeD is our next work to do.

Activated HSCs are the major source of ECM production in the liver fibrosis and their activation results from the inflammatory activity of liver immune cells, predominantly macrophages. We found that cbFeD remarkably attenuated

the recruitment of leukocytes and the number of F4/80 positive Kupffer cells also reduced significantly. Meanwhile, the number of cells that express a-SMA and desmin, markers of HSC activation, decreased dramatically upon cbFeD treatment in our experiment. cbFeD has long been found to exert an immunomodulatory effect and our results have revealed an obvious anti-inflammatory effect of cbFeD in the fibrogenic liver via reducing inflammatory cell recruitment and activation [21,22]. The direct effect of cbFeD extracts on the activation of HSCs in vitro has also been investigated and further revealed a dose-dependent inhibition on TGF-β 1 induced HSC proliferation and activation. Since cbFeD is known to have a wide range of pharmacological effects and water extracts of cbFeD contain multiple nutrients and chemical components, the main active component of cbFeD and the exact action mechanism awaits further investigation.

As the liver is exposed to microbial products derived from the gut, the microbiota in the gut participates in the activation of inflammatory pathways and fibrogenesis of the liver. [36–39] cbFeD is well recognized for its bowel relaxing effect and widely taken as an anti-constipation food beyond being used as a tonic. We previously evaluated gut dysbiosis in a constipated mouse model and found that the application of cbFeD modulated abundance of Deferribacteres [40,41]. Whether gut microbiota plays a role in the beneficial effect of cbFeD in liver fibrogenesis awaits investigation.

In conclusion, cbFeD was able to attenuate liver injury and alleviate liver fibrogenesis in $CCl_4$-treated mice through attenuating intrahepatic oxidative stress, reducing hepatocyte apoptosis, suppressing inflammatory cell recruitment, and inhibiting activation of HSCs. Our research revealed a potential

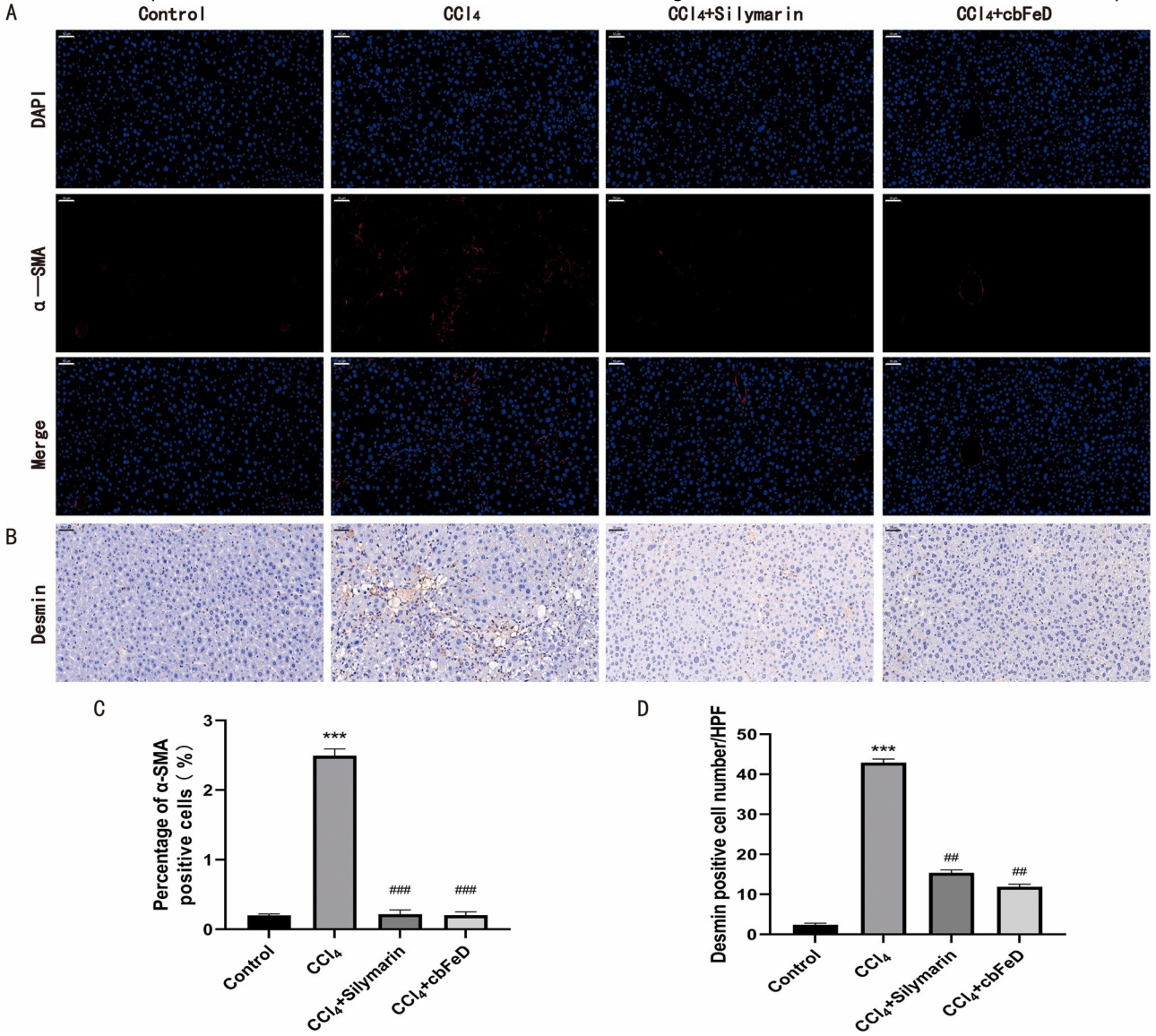


**Fig. 8.** cbFeD inhibited the activation of HSCs in liver. (A) Expression of α-SMA in the liver tissues from each group were assessed by immunofluorescence. (B) Expression of desmin were detected using IHC staining of liver sections. Magnification ×200; Scale bar = 50 μm. (C) The percentage of a-SMA positive cells was calculated as the number of positive stained cells dividing the total number of cells counted under 5 randomly selected HPF for each sample and 4 samples per group were assessed. (D) The percentage of desmin positive cells was calculated under 5 randomly selected HPF for each sample and 4 samples per group were assessed. Results are expressed as the mean ± SEM; (***) $P < 0.001$, significantly different compared to the control group; (##) $P < 0.01$, significantly different compared to the $CCl_4$ group; (###) $P < 0.01$, significantly different compared to the $CCl_4$ group.

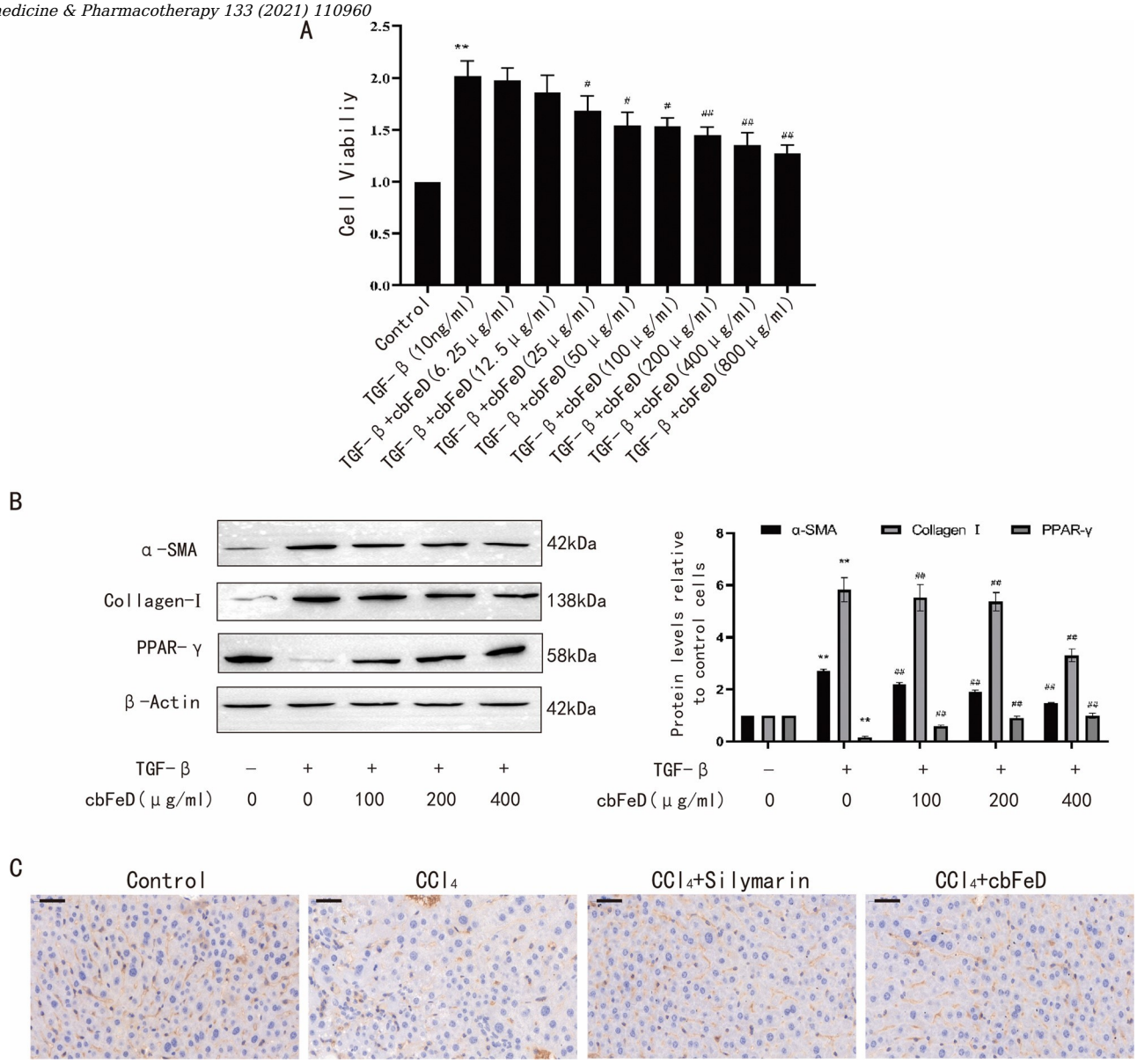


**Fig. 9.** cbFeD inhibits TGF-β1-induced hepatic stellate cells (HSCs) activation. (A) LX2 cells were treated with TGF-β1 (10 ng/mL) and water extract of cbFeD at indicated concentrations for 24 h. Cell viability was assessed. Data are presented for three independent experiments, with similar results. (*) $p < 0.05$, (**) $p < 0.01$ vs. control group. (#) $p < 0.05$, (##) $p < 0.01$ vs. TGF-β1 alone group. (B) LX2 cells were treated with TGF-β1(10 ng/mL) and water extract of cbFeD with indicated concentrations for 24 h. Western blot analyzed the protein levels of α-SMA, Collagen-I and PPAR-γ. The values were represented by means ± SD at least 3 separate experiments. (*)$P < 0.05$, (**)$P < 0.01$compared to control group. (#) $P < 0.05$, (##) $P < 0.01$ compared to TGF-β1 induced group. (C) Representative images of immunohistochemical staining of PPAR-γ in liver tissues from each treatment group. The black bar represents a length of 50 μm.

use of cbFeD in the prevention and treatment of hepatic fibrosis.

## Author contributions

Conceived and designed the experiments: Yunpeng Luan, Huaning Wang, Junbo Hu, Zhuoya Li

Performed the experiments: Xiang Li, Yue Xing, Dechang Mao, Mei Xu, Lu Ying, Yunqi Luan, Hongmin Wang, Chunyan Li, Yanmei Li, Shuangqing Zheng, Zhipeng Li

Analyzed the data: Xing Yue, Dechang Mao, Lu Ying, Yunqi Luan

Wrote the paper: Xiang Li, Yue Xing, Dechang Mao, Yunpeng Luan, Huaning Wang, Junbo Hu, Zhuoya Li

## Funding

This study was funded by National Natural Science Foundation of China (NSFC) (31860254), Advanced and Characteristic Key Biological Disciplines of Yunnan Province (project serial code: 50097505), and Scientific and Techenological Innovation Team Construction Project for Protection and Utilization of Under-forest Biological Resources (project serial code: 51400605).

## Declaration of Competing Interest

Authors have no conflict of interest to declare.

## References

[1] R. Bataller, D.A. Brenner, Liver fibrosis, J. Clin. Invest. 115 (2) (2005) 209–218.
[2] J. Liu, W. Liang, W. Jing, et al., Countdown to 2030: eliminating hepatitis B disease, China, Bull. World Health Organ. 97 (3) (2019) 230.
[3] J.G. Fan, G.C. Farrell, Epidemiology of non-alcoholic fatty liver disease in China, J. Hepatol. 50 (1) (2009) 204–210.
[4] V. Hernandez-Gea, S.L. Friedman, Pathogenesis of liver fibrosis, Annu. Rev. Pathol.
Mech. Dis. 6 (2011) 425–456.
[5] T. Kisseleva, D.A. Brenner, Role of hepatic stellate cells in fibrogenesis and the reversal of fibrosis, J. Gastroenterol. Hepatol. 22 (2007) S73–S78.
[6] I. Mederacke, C.C. Hsu, J.S. Troeger, et al., Fate tracing reveals hepatic stellate cells as dominant contributors to liver fibrosis independent of its aetiology, Nat.
Commun. 4 (2013) 2823.
[7] K. Iwaisako, C. Jiang, M. Zhang, et al., Origin of myofibroblasts in the fibrotic liver in mice, Proc. Natl. Acad. Sci. 111 (32) (2014) E3297–E3305.
[8] S.L. Friedman, Hepatic stellate cells: protean, multifunctional, and enigmatic cells of the liver, Physiol. Rev. 88 (1) (2008) 125–172.
[9] E.A. Tsochatzis, J. Bosch, A.K. Burroughs, Liver cirrhosis, Lancet 383 (9930) (2014)
1749–1761.
[10] M. Pinzani, Pathophysiology of liver fibrosis, Dig. Dis. 33 (4) (2015) 492–497.
[11] S.S. Thorgeirsson, J.W. Grisham, Molecular pathogenesis of human hepatocellular carcinoma, Nat. Genet. 31 (4) (2002) 339.
[12] R. Feng, X. Yuan, C. Shao, et al., Are we any closer to treating liver fibrosis (and if no, why not)? J. Dig. Dis. 19 (3) (2018) 118–126.
[13] E.L. Ellis, D.A. Mann, Clinical evidence for the regression of liver fibrosis, J. Hepatol. 56 (5) (2012) 1171–1180.
[14] M. Pinzani, K. Rombouts, Liver fibrosis: from the bench to clinical targets, Dig.
Liver Dis. 36 (4) (2004) 231–242.
[15] P. Wang, Y. Koyama, X. Liu, et al., Promising therapy candidates for liver fibrosis, Front. Physiol. 7 (2016) 47.
[16] Z.J. Chen, Q.H. Wei, J.Y. Zhou, Research progress of Codonopsis foetens, Yunnan Journal of Traditional Chinese Medicine and Materia Medica. 27 (4) (2006) 49–50.
[17] R.L. Yang, C.L. Zhu, Pharmacodynamic study and acute toxicity test of Codonopsis bulleyana Forrest, Journal of Yunnan University of Traditional Chinese Medicine.
22 (3) (1999) 4–7.
[18] P.H. Liu, M.Y. Liu, Y.G. Zhang, S.R. Lu, Study on nutritional components of Codonopsis bulleyana forrest, Journal of Yunnan agricultural university (Natural Science) 30 (2015) 418–423.
[19] Y. Luan, D. Mao, A. Guo, et al., The effect of Codonopis bulleynana Forest ex Diels on chronically constipated mice, Saudi J. Biol. Sci. 26 (2) (2019) 402–412.
[20] Y. Yang, X.Y. Hu, Q. Sang, Y.X. Cheng, Influence of compound chinese medicine containing Codonopsis pilosula produced in Yunnan Province on purgation and its primary action mechanism, Journal of Yunnan University of Traditional Chinese Medicine 40 (5) (2017) 18–22.
[21] X.F. Zhang, M.Y. Zhang, M.C. Shi, H. Zhang, H.C. Ren, Clinical Observation of the effect of Tsoong on 40 Cases of Deficiency Syndrome in Middle-and old aged patients, Yunnan Journal of Chinese Traditional Medicine. 12 (6) (1991) 26–27.
[22] Z.J. Chen, Y.S. Li, Q.H. Wei, et al., Efects of Codonopis bulleynana Forest ex Diels on enhancing sensitivity, reducing toxicity of chemotherapy and regulating immune function in Sarcoma 180 tumor-bearing mice, Chin Trad Patent Med 34
(2012) 1848–1851.
[23] Y.P. Luan, Q.F. Li, S.G. Wu, et al., Tsoong induces apoptosis and inhibits proliferation, migration and invasion of pancreatic ductal adenocarcinoma cells, Mol. Med. Rep. 17 (3) (2018) 3527–3536.
[24] Y. Luan, Y. Li, L. Zhu, et al., Codonopis bulleynana Forest ex Diels inhibits autophagy and induces apoptosis of colon cancer cells by activating the NF-κB signaling pathway, Int. J. Mol. Med. 41 (3) (2018) 1305–1314.
[25] M.K. Manibusan, M. Odin, D.A. Eastmond, Postulated carbon tetrachloride mode of action: a review, Journal of Environmental Science and Health Part C 25 (3) (2007)
185–209.
[26] P. LIU, Y. HUANG, Y. JIN, et al., The content measurement and anti-oxidant activity of polysaccharides from Codonopsis bulleyana Forrest ex Diels, Food Sci. Technol. 8 (2013) 77.
[27] X.Z. Li, Y.M. Yan, X.C. Zhuang, Y.X. Cheng, Compounds from Codonopsis pilosula Produced in Xundian of Yunnan Province, Nat Prod Res Dev 29 (2017) 1858–1866.
[28] P.G. Pietta, Flavonoids as antioxidants, J. Nat. Prod. 63 (7) (2000) 1035–1042.
[29] S. Kumar, A.K. Pandey, Chemistry and biological activities of flavonoids: an overview, The Scientific World Journal 2013 (2013).
[30] P.H. Liu, Y.R. Jin, M.Y. Liu, et al., Total flavonoids and antioxidant activity of aerial parts of Codonopsis bulleyana, Southwest China Journal of Agricultural Sciences 27 (5) (2014) 1894–1898.
[31] P. LIU, X. XU, L. LI, et al., Extraction, speration and antioxidation of flavonoids from aerial parts of Codonopsis bulleyana, Food Sci. Technol. 2 (2018) 46.
[32] F.Y. Qin, L.Z. Cheng, Y.M. Yan, et al., Choushenosides AC, three dimeric catechin glucosides from Codonopsis pilosula collected in Yunnan province, China, Phytochemistry 153 (2018) 53–57.
[33] F.Y. Qin, L.Z. Cheng, Y.M. Yan, et al., Two novel proline-containing catechin glucoside from water-soluble extract of Codonopsis pilosula, Molecules 23 (1) (2018) 180.
[34] X.Y. Hu, F.Y. Qin, X.F. Lu, et al., Three new polyynes from Codonopsis pilosula and their activities on lipid metabolism, Molecules 23 (4) (2018) 887.
[35] X.Z. Li, L.Z. Cheng, Y.M. Yan, et al., SIRT1 inhibitory compounds from the roots of Codonopsis pilosula, J. Asian Nat. Prod. Res. 21 (1) (2019) 25–32.
[36] B.C. Davis, J.S. Bajaj, The human gut microbiome in liver diseases[C]//Seminars in liver disease, Thieme Medical Publishers 37 (02) (2017) 128–140.
[37] H. Tilg, P.D. Cani, E.A. Mayer, Gut microbiome and liver diseases, Gut 65 (12)
(2016) 2035–2044.
[38] J. Boursier, O. Mueller, M. Barret, et al., The severity of nonalcoholic fatty liver disease is associated with gut dysbiosis and shift in the metabolic function of the gut microbiota, Hepatology 63 (3) (2016) 764–775.
[39] S.R. Sharpton, V. Ajmera, R. Loomba, Emerging role of the gut microbiome in nonalcoholic fatty liver disease: from composition to function, Clin. Gastroenterol. Hepatol. 17 (2) (2019) 296–306.
[40] Y. Luan, D. Mao, A. Guo, et al., The effect of Codonopis bulleynana Forest ex Diels on chronically constipated mice, Saudi J. Biol. Sci. 26 (2) (2019) 402–412.
[41] Y. Li, Y. Luan, X. Yue, et al., Effects of Codonopis bulleynana Forest ex Diels on Deferribacteres in constipation predominant intestine tumor: Differential analysis, Saudi J. Biol. Sci. 26 (2) (2019) 395–401.